COMPUTER-AIDED CIVIL AND INFRASTRUCTURE ENGINEERING

Computer-Aided Civil and Infrastructure Engineering **30** (2015) 508–523

Simulation-Based Seismic Risk Assessment of Gas Distribution Networks

Simona Esposito, Iunio Iervolino*, Anna d'Onofrio & Antonio Santo

Università degli Studi di Napoli Federico II, Via Claudio 21, 80125, Naples, Italy

Francesco Cavalieri & Paolo Franchin

Università degli Studi di Roma La Sapienza, Via Gramsci 53, 00197, Rome, Italy

Abstract: *The basic function of a gas distribution system, essentially composed of buried pipelines, reduction stations, and demand nodes, is to deliver gas from sources to end users. The objective of the article is to discuss the evaluation of seismic risk of gas networks in compliance with the performance-based earthquake engineering framework adapted to spatially distributed systems. In particular, three issues are addressed: (1) spatial seismic hazard characterization in terms of ground shaking and permanent ground deformation; (2) analysis of system's vulnerability via fragility curves; (3) seismic performance evaluation via computer-aided simulation. As an application, the seismic risk analysis of L'Aquila (central Italy) gas distribution network, a 621-km mid- and low-pressure pipeline system was considered. The analyses were performed with reference to the mid-pressure part of the network, through an object-oriented software, specific for risk assessment of lifelines, developed by the authors. Results in terms of connectivity-based performance indicators are presented and discussed, along with a performance disaggregation analysis carried out to evaluate the contribution of the components of the system to the risk.*

1 INTRODUCTION

Lifelines are those utility systems essential for communities; examples are the telecommunication, transportation, power, water, and gas networks. Disruption of lifelines caused by earthquakes can have an impact both in the short term, for emergency management issues, and in the long term, for the effects on the economy and social stability of the served region. This explains why the evaluation of seismic reliability of these systems has attracted attention in recent years (e.g., Banerjee and Shinouzuka, 2004; Pitilakis et al., 2006; Adachi and Ellingwood, 2008, 2009; Wang et al., 2010; Cavalieri et al., 2014).

The study presented in the following focuses on gas distribution systems, to which past earthquakes caused a significant amount of damage, especially to its main component, that is buried pipelines (O'Rourke and Palmer, 1996). The 1971 San Fernando earthquake (moment magnitude, M_w, 6.7) caused damage to underground welded-steel transmission pipelines. The 1923 Kanto (M_w 7.9) earthquake caused several breaks to gas pipelines in the Tokyo region. Damages to aboveground support facilities have also been observed in past events (FEMA, 1992), especially in the case of inadequate anchorage of equipment.

A gas distribution system comprises two main categories of components: (i) a number of point-like critical facilities (reduction stations and groups where gas is pressurized/depressurized and/or measured); and (ii) pipelines constituting the distribution network.

The causes of earthquake damage to components of gas distribution systems include large permanent soil deformations produced by fault displacements, landslides, liquefaction of sandy soils, associated lateral spreading, and ground settlements, as well as ground shaking associated with traveling seismic waves. The latter case is often referred to as transient ground deformation (TGD), while the former is generally synthesized as permanent ground deformation (PGD); i.e., the *geotechnical hazard*. These phenomena affect both aboveground and buried components. However, in the

*To whom correspondence should be addressed. E-mail: *iunio.iervolino@unina.it*.

DOI: 10.1111/mice.12105

case of buried pipelines, PGD is especially important (O'Rourke and Liu, 1999).

Because this kind of system is extended in space, a key difference with respect to seismic risk analysis of point-like facilities is that the seismic hazard has to be evaluated jointly for all the locations of the system's components. Moreover, the performance evaluation of lifelines, related to the level of service, reflects their spatially distributed and functionally interconnected nature, which needs specific indicators.

Even if nonsampling-based approaches have been developed (e.g., Kang et al., 2008; Kim and Kang, 2013; Duenãs-Osorio and Rojo, 2011), the listed complexities and the need to account for all the uncertainties involved in the seismic risk analysis of gas networks favor probabilistic assessment procedures based on computer-aided Monte Carlo simulation (or MCS; e.g., Jahani et al., 2014). In turn, MCS may be computationally demanding depending on the modeling of the system of interest and/or on the order of magnitude of the probabilities to estimate (e.g., Pinto et al., 2004). These issues, motivating the study herein presented, render the probabilistic seismic risk evaluation peculiar and relatively less consolidated with respect to that of buildings for which the performance-based earthquake engineering (PBEE) framework was originally set. In fact, the study aimed at evaluating the seismic risk of a gas distribution network, following the principles and objectives of PBEE and considering all the issues involved, using as much as possible state-of-the art tools. To this aim, the work includes the probabilistic characterization of seismic input, the definition of vulnerability of the network's components, the analysis of the system's seismic performance measures, and finally the probabilistic simulation for risk assessment.

As an illustrative, yet real, application, the mid-pressure (MP) part of the L'Aquila (central Italy) gas distribution system is considered. It is characterized by three reduction stations connecting the network to the high-pressure (HP) nationwide network, more than 200 km of pipelines either made of steel or high-density polyethylene (HDPE) pipes, and about 200 reduction groups (RGs). Detailed information about the system was available for this network, including performance in the 2009 M_w 6.3 earthquake (Esposito et al., 2013) due to a partnership with its operator (Enel Rete Gas s.p.a.).

For the purposes of seismic risk assessment, a single earthquake fault, the Paganica fault (Pace et al., 2006), is considered (and in this sense, the analysis is conditional to this assumption). It is beneath the region served by the network and it is believed to have generated the 2009 L'Aquila earthquake. The reason for such a choice is twofold: (i) it is expected to dominate the hazard for the gas system; and (ii) the study is methodological, more faults would not add to it.

Seismic risk is herein expressed in terms of probability of exceedance of service disruption levels, measured by connectivity-based performance indicators (PIs), given the occurrence of an earthquake on the considered fault that may be converted in performance rate. Indeed, the performance rate can be translated in monetary terms, which is common in risk assessment, once the expected loss given PI is available, yet this was outside the scope of the study.

Analyses were carried out with a purpose-made object-oriented model of interconnected infrastructural systems (Franchin and Cavalieri, 2013), within which the authors have specifically developed a prototype software for the seismic risk assessment of gas systems.

The article is structured such that Section 2 describes the general framework for the probabilistic seismic performance assessment of gas distribution networks. Section 3 discusses the hazard characterization of the region, the fragility selection, and the seismic performance simulation procedure. Moreover, details on the implementation of the prototype software are also provided. Subsequently, the analysis of the network is discussed (Section 4) and results in terms of PIs are finally presented and discussed.

2 ISSUES IN THE PERFORMANCE-BASED SEISMIC RISK ASSESSMENT OF GAS SYSTEMS

2.1 Seismic hazard characterization

This section describes the general process to characterize the seismic input (in terms of TGD and PGD) acting on the components of a gas network. In particular, the principal differences with respect to single-site systems are pointed out for both phenomena and referring to pipelines and stations, which are the main components of the lifeline under study.

2.1.1 TGD. During an earthquake, wave propagation causes transient vibratory soil deformations over a wide geographic area. Ground motion effects are usually described in terms of peak ground motion intensity measures (*IMs*); e.g., peak ground acceleration, PGA, or peak ground velocity, PGV, that may be evaluated, conditional to earthquake features such as magnitude and source-to-site distance, using a ground motion prediction equation (GMPE).

Since a gas system generally covers a large area, the first aspect to consider in the seismic input modeling is that the latter is composed of large vectors of ground

motion intensities (for all sites in the region where the system deploys). This means that seismic hazard has to be represented in terms of random fields (e.g., Park et al., 2007; Adachi and Ellingwood, 2009; Zerva, 2009; Esposito and Iervolino, 2011). This is a peculiar feature differing from the seismic risk analysis of point-like facilities. In fact, if probabilistic assessment of ground motion at two or more sites at the same time is of concern, a spatial correlation model, accounting for the statistical dependencies between *IMs* as a function, for example, of intersite separation distance, is needed. This serves to model the joint probability density function (JPDF) of *IMs* at all locations. A common model (e.g., Jayaram and Baker, 2009) assumes that the JPDF of the logarithm of *IMs* at a number of sites is a multivariate normal distribution, the mean vector of which is provided by a GMPE and the covariance matrix reflects correlation of residuals (to follow).

Still on the TGD side, it has to be considered that the performance of spatially distributed systems may be conditional upon the failure of many different components, each of which may be characterized by fragility curves that are a function of different *IMs*. For example, some elements of a gas system, such as regulator stations, have fragility curves typically expressed in terms of PGA, while fragility of pipelines may be function of PGV. Because *IMs* at the same site, generally, are not independent of each other, this raises another issue: the probabilistic seismic input representation has also to account for the cross-correlation between the *IMs*. To address this, the *conditional hazard* approach may be considered (Iervolino et al., 2010). It consists of obtaining the conditional distribution of a secondary measure IM_2 (e.g., PGV) at a site, given the occurrence of a primary measure, IM_1, at the same site (e.g., PGA), $f_{IM_2|IM_1}(im_2|im_1)$. If the random field for IM_1 accounts for the spatial correlation, the random field conditionally obtained for IM_2 also implicitly accounts for it. The simplest application of conditional hazard requires site–specific correlation coefficients between *IMs* and acceptability of the hypothesis of joint normality of the logarithms of the primary and secondary *IMs*. Therefore, for a generic system characterized by N sites and two *IMs*, instead of characterizing the joint distribution of all sites and ground motion parameters of interest, it is necessary just to model the JPDF of IM_1 and then the conditional distribution of the secondary *IM* at each site. The approach is shown in Figure 1, for a simplified system deployed in three sites.

Note that this approach assumes that IM_1 at a site is *sufficient* (i.e., Luco and Cornell, 2007) for IM_2 at the same site, that is, IM_2 is independent of any other ground motion parameter given IM_1 and that the dependence of the variable IM_2 on the variable IM_1 is limited to the colocated primary variable (see also Weatherill et al., 2014).

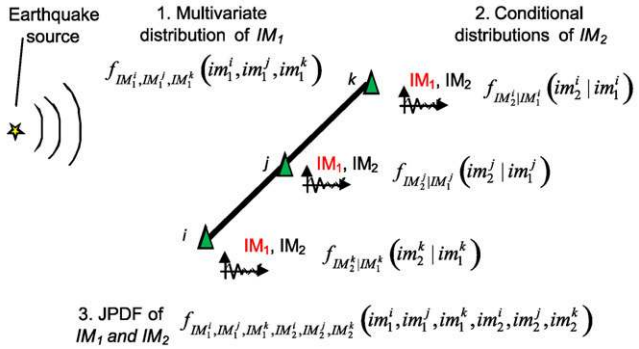

Fig. 1. Sketch of the procedure to model the joint distribution of cross-correlated *IMs* via conditional hazard.

2.1.2 PGD. Buried components (i.e., pipelines) require the consideration of PGD hazard. Although PGDs are usually limited to small regions, their damage potential may be significant. The principal causes of PGD are (Kramer, 1996): (i) coseismic fault displacement in the near-fault area; (ii) liquefaction-induced lateral spreading, and seismic settlement; (iii) landslides triggered by seismic shaking.

The relative impact of the various earthquake-induced PGDs on a pipeline system depends on the morphologic, geological, and geotechnical conditions of the subsoil. In general, fault displacement is often evaluated by means of semiempirical relations that correlate displacement to the magnitude of the earthquake (e.g., Petersen et al., 2011), while for liquefaction and landsliding, the amount of resulting displacement may be evaluated through models relating a parameter representing the latter to a ground motion intensity measure. In this context, the simple approach of HAZUS (FEMA, 2004), requiring limited information about the geotechnical characterization of the region, may fit the purpose of the risk analysis of large systems, as gas networks are. According to HAZUS, the first step of liquefaction hazard evaluation is the determination of *liquefaction susceptibility*. The next stage is to determine the likelihood that an earthquake will be able to initiate the phenomenon (i.e., the probability of liquefaction). Finally, given that liquefaction occurs at a particular location, the amount of PGD (i.e., displacement) may be predicted via models such as those by Youd et al. (2002).

Similar to liquefaction, the characterization of slope displacement starts generally from the evaluation of landslide susceptibility. It is related to the morphologic and groundwater conditions of the area, as well as to the geologic origin and the strength characteristics

of soils. These factors contribute to the determination of the critical acceleration k_c that is the minimum shaking intensity required to overcome the slide resistance of the slope.

In the HAZUS procedure, the critical acceleration is related to a 10-point susceptibility scale based on the local lithology, the slope angle, and groundwater conditions, without any reference to direct measurements of the soil strength parameters. The groundwater condition is divided into dry conditions (groundwater below level of the sliding) or wet conditions (groundwater level at ground surface). Hence, in a susceptible deposit and for a given earthquake, permanent displacements either occur or not depending on whether the induced peak ground acceleration at surface, PGA_s, exceeds k_c. Once the landslide occurs, the calculation of the expected ground displacement may be carried out via models such as that by Saygili and Rathje (2008).

As mentioned, the HAZUS approach is believed to represent a base-level scale-compatible application of geotechnical hazard characterization in the context of probabilistic seismic risk analysis of spatially distributed systems due to the limited data required. In fact, in the case where more detailed geotechnical data are available for the region of interest, refined procedures could be considered (e.g., Baker and Faber, 2008; Kramer, 1996). However, it has to be recalled that the geotechnical hazard in probabilistic risk assessment of infrastructures is not a consolidated issue yet; see Weatherill et al. (2014) for a discussion.

2.2 Vulnerability

To estimate seismic damage for a natural gas distribution system given ground shaking or ground deformation, earthquake intensity parameters have to be related to the effects by means of fragility functions for components. In particular, for point-like elements, these relations typically provide the probability of reaching or exceeding some damage state (DS) given the intensity. This applies to the aboveground components of a gas distribution network, while for pipelines, the fragility models usually consist of a seismic-intensity-dependent rate, providing the number of damages (e.g., leaks or breaks) per unit length.

2.2.1 Stations. In a gas distribution system, three main types of point-like facilities may exist:

1. metering/pressure reduction stations (M/R stations) that contain metering equipment for monitoring and measuring the gas flow, and reduction lines for reducing the gas pressure before its distribution into the medium pressure pipe system;
2. RGs, where the gas pressure is reduced as required to be delivered to the end user;
3. metering stations that are only flow measurement points.

Considering that stations comprise the shelter and the equipment inside, they may be classified with respect to different aspects: building typology; anchored or unanchored subcomponents; or electrical and mechanical components (Gehl et al., 2014).

Although in the literature, no fragility curves are available for these components, some authors (e.g., Chang and Song, 2007) assume that at least the M/R stations can be characterized with the same fragility features of compressor stations, in terms of lognormal cumulative distribution functions. DSs and fragility curves for compressor stations (e.g., those in FEMA, 2004) are usually a function of PGA, and sometimes PGD, if located in liquefiable or landslide-prone areas.

2.2.2 Buried pipelines. As mentioned, buried pipelines are sensitive to PGD, in addition to TGD due to seismic wave propagation. Among the various seismic parameters used to correlate the ground shaking effects to the damage suffered by buried pipelines, PGV is often preferred (O'Rourke et al., 1998).

In the case of pipeline components, fragility curves available in literature are usually based on empirical data collected in past earthquakes. These semiempirical models are mostly based on the recorded number of repairs collected from field crews (e.g., ALA, 2001; Eidinger, 1998; O'Rourke and Ayala, 1993). Semiempirical models do not explicitly discriminate all the possible failure modes of buried pipelines subjected to transient and ground deformation, whereas it is acknowledged that they may be related to shape discontinuities of the pipelines as well as sharp variations in strength and stiffness characteristics of the soil. As a result, all fragility relations for pipelines are given in terms of the repair rate, R_R, per unit length of pipe. The main factors affecting the vulnerability of pipelines, usually accounted for in the formulation of the repair rate, are pipe material, pipe diameter, and pipe connection type. Then, using a Poisson probability distribution and R_R as its parameter, one can assess the probability of having any number of damages in a pipe segment, given the local intensity.

According to HAZUS, two DSs may be considered for pipelines: leaks and breaks. When a pipe is damaged due to ground failure, it is assumed that the proportions of leaks and breaks are 0.2 and 0.8, respectively; whereas for ground shaking, leaks and breaks proportions are 0.8 and 0.2, respectively.

2.3 Performance

2.3.1 Gas network models and analyses. The seismic performance analysis of a gas network (and of lifeline systems in a more general sense) can be carried out at two main levels:

1. *connectivity-based,* related to the existence of a path connecting sources to demand nodes (in a system where both links and nodes may fail) allowing the assessment of serviceability in terms of, for example, the number of distribution nodes that remain accessible from at least one supply node after the earthquake;
2. *flow-based*, that considers the network's capacity and takes into account additional factors/constraints in the assessment of serviceability; e.g., the minimum pressure at each demand node.

Depending on the purpose of the analysis, different methods and tools can be used for the evaluation of seismic performance of gas networks. Connectivity analysis requires a simple description of the system in terms of a graph, defined as a collection of nodes (divided into sources or stations, sinks or demand nodes, and joints) and links (i.e., pipes) connecting nodes. Connectivity analysis tools are limited to those of graph theory (e.g., Ching and Hsu, 2007). These algorithms are applied to the network after removing the parts of the system that failed after the seismic event.

In flow-based analysis, the network performance is measured evaluating the actual flow delivered to end users, as a function of the pressure at demand nodes. For the purpose of calculating pipe flow and nodal pressure before and after the seismic event, it is necessary to consider flow equations (the application of flow equations is required for the calculation of the pressure drop along the network) and a method to solve the network analysis problem (see Osiadacz, 1987, for a discussion). Also, in this case, the analysis should be performed on the network after removing the damaged parts of the system.

2.3.2 PIs. Depending on the connectivity-based or flow-based goal of the analysis, different PIs may be evaluated. Moreover, PIs can refer to the component-level or the system-level.

For a gas network, two possible system-level PIs for connectivity analysis are the *serviceability ratio* (SR) and the *connectivity loss* (CL). The former, originally defined for water supply systems (Adachi and Ellingwood, 2008), is directly related to the number of distribution nodes in the utility network that remain accessible from at least one supply facility after the earthquake.

The latter index, defined by Poljanšek et al. (2012), was considered for the purpose of this study and measures the average reduction in the ability of demand nodes to receive flow from source nodes.

In each earthquake event, SR may be computed as in Equation (1), where w_i is a weighting factor assigned to the distribution node i (i.e., the nominal flow of the RG demand node), X_i represents the functionality of ith demand node, which is modeled as the outcome of a Bernoulli trial (i.e., $X_i = 1$ if the node is accessible from at least one supply facility and zero otherwise), and n is the number of distribution nodes.

$$SR = \sum_{i=1}^{n} (w_i \cdot X_i) \Big/ \sum_{i=1}^{n} w_i \tag{1}$$

CL is computed as in Equation (2), counting the number of source nodes connected to the ith demand node in the original (undamaged) network $N^i_{\text{source,orig}}$ and then in the damaged network $N^i_{\text{source,dam}}$, where $\langle\ \rangle$ denotes averaging over all demand nodes.

$$CL = 1 - \left\langle \frac{N^i_{\text{source,dam}}}{N^i_{\text{source,orig}}} \right\rangle_i \tag{2}$$

For a more extended discussion on other possible PIs for gas networks, see Esposito (2011).

3 PROCEDURE FOR SIMULATION-BASED SEISMIC RISK ANALYSIS OF GAS DISTRIBUTION NETWORKS

Due to the articulation of the general issues discussed in the previous section, the seismic risk analysis of gas networks is more profitably illustrated via its implementation. Therefore, although remaining on the methodological side, this section describes the steps of the simulation-based assessment, considering all the aspects described above, as applied to the MP portion of the L'Aquila gas distribution system. Five principal steps may be identified in the analysis:

1. probabilistic TGD characterization starting from an event randomly originated on the considered fault, and including spatial correlation of ground motion;
2. probabilistic characterization of the PGD hazard as a function of TGD, focusing on seismically induced landslides (requires the geotechnical characterization of the network area);
3. probabilistic characterization of earthquake damage to each component within the network via fragility models;

4. system's performance analysis via a connectivity algorithm to integrate the damage of stations and pipelines to evaluate the systemic damage;
5. probabilistic risk assessment via MCS.

The simulation was performed implementing the application network in the *object-oriented framework for infrastructure modeling and simulation* (OOFIMS) software, developed according to the *object-oriented paradigm* (OOP). The latter is commonly adopted in engineering studies requiring numerical analysis and design of large systems (e.g., Chuang and Adeli, 1993; Yu and Adeli, 1993; Hung and Adeli, 1994; Adeli and Yu, 1995; Karim and Adeli, 1999a, b; Jiang and Adeli, 2004; Adeli and Kao, 1996), as it will be briefly discussed in Section 3.3.

3.1 L'Aquila MP gas distribution system

In the L'Aquila region (central Italy), the gas is distributed via a 621-km pipeline network, 234 km of which with gas flowing at mid pressure (2.5–3 bar), and the remaining 387 km with gas flowing at low pressure (0.025–0.035 bar).

The MP distribution network is connected to the HP transmission network (deployed at a national level) through three M/R stations. These are cased in one-story reinforced concrete structures hosting internal regulators and mechanical equipment (heat exchangers, boilers, and bowls), where the gas undergoes the following processes: (1) gas preheating; (2) gas pressure reduction and regulation; (3) gas odorizing; and (4) gas pressure measurement.

Pipelines of the distribution network are either made of steel or HDPE. The latter pipes have nominal diameters ranging from 32 to 400 mm, whereas the diameter of the steel pipes is usually between 25 and 300 mm. Before 1990, steel pipes were generally characterized by gas-welded joints, whereas, more recently, gas-welded joints are used for diameter less than 250 mm and arc-welded joints are used otherwise. HDPE pipes feature fusion joints. Construction years of the analyzed network range from 1968 to 2009 and the burial depth was usually between 0.6 and 0.9 m before 1992, and equal to 1 m thereafter.

The transformation of the MP into the low distribution pressure (LP) is operated via 300 RGs that are buried, sheltered in a metallic kiosk, or housed within/close to a building. Several demand nodes (referred to as IDU, *impianto di derivazione utenza* in Italian), consisting of buried and aboveground pipes and accessory elements, allow the supply of natural gas to end users, from LP network. For large users, such as industrial facilities, the demand node is located along the MP network.

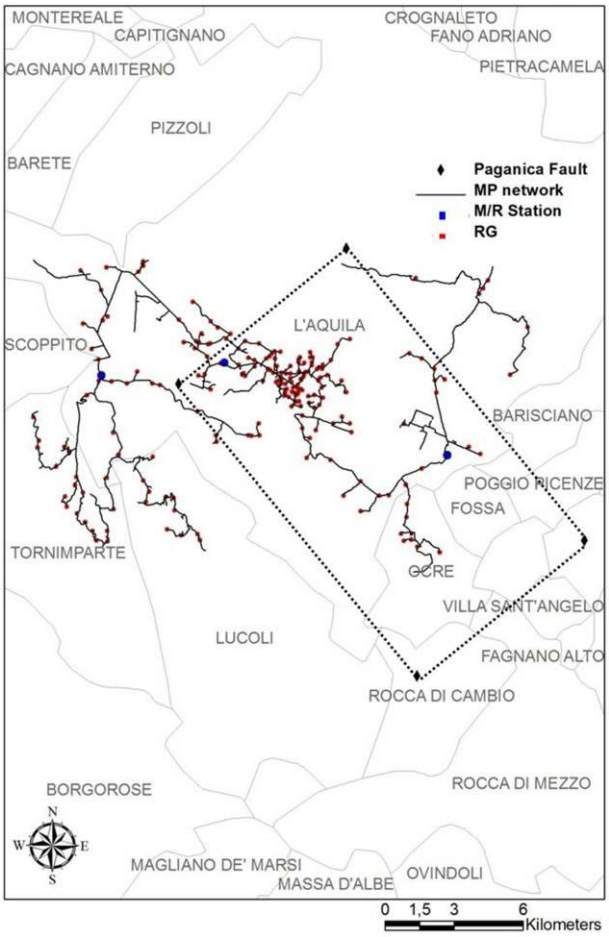

Fig. 2. Application network (L'Aquila, central Italy).

Collaboration with the network's operator enabled the characterization of the system via a *geographic information system*, developed for the purpose of the study and reporting data on physical and operational characteristics.

The MP portion of the system selected for the study (Figure 2) includes the three M/R stations, 209 RGs, and pipelines at mid pressure.

3.2 Procedure

As mentioned, a simulation-based connectivity analysis was the object of this study. Considering that the function of a gas network at MP is to deliver gas to RGs, the network performance was assessed evaluating the availability of end nodes (RGs) of the L'Aquila system.

Both TGD and PGD hazards were evaluated. Pipelines and M/R stations were considered the

vulnerable elements within the network, and the risk assessment was performed in terms of two PIs.

In the following subsections, a description of the adopted methodology and models is provided.

3.2.1 Regional seismic intensity simulation. The process to compute the seismic input, in terms of TGD and PGD in each simulation run, is essentially divided into five separate stages:

1. sampling of the event on the considered seismic fault;
2. sampling of the random field of the primary *IM* at bedrock (PGA_r);
3. conditional sampling of the secondary *IM* at bedrock (PGV_r);
4. amplification due to local site conditions to get PGA_s and PGV_s that are the *IMs* at the surface;
5. sampling of displacement consequential to PGD due to landslide.

1. The Paganica fault (normal faulting style) was considered for the generation of characteristic earthquakes of (fixed) moment magnitude equal to 6.3 and return period equal to 750 years (Pace et al., 2006). Uncertainty around the characteristic magnitude, if any, was neglected. Also, the referenced study only provides a single magnitude for the fault. Data on fault geometry (Figure 2) used herein are those of Chioccarelli and Iervolino (2010). Given the magnitude, the simulation of the event on the fault was in terms of epicentral location, which was assumed as uniformly distributed. To this aim, the fault was discretized as a lattice (see also Weatherill et al., 2014).
2. The ground motion intensity for the primary *IM* was evaluated using a GMPE on a regular grid of points discretizing the region covered by the gas network, as expressed in Equation (3):

$$\log Y_{pj} = \overline{\log Y_{pj}}(M, R, \underline{\theta}) + \eta_j + \varepsilon_{pj} \tag{3}$$

where Y_{pj} denotes the *IM* at a site p due to earthquake j; $\overline{\log Y_{pj}}(M, R, \underline{\theta})$ is the mean of its logarithm, conditional to magnitude (M), source-to-site distance (R) and other parameters ($\underline{\theta}$), η_j is the interevent residual, and ε_{pj} is the intraevent heterogeneity of ground motion. The interevent term, common to all sites, represents the systematic deviation of the specific earthquake from the GMPE, and it is usually assumed as a normally distributed random variable with zero mean and standard deviation σ_{inter} (again, from the GMPE model). ε_{pj} is the remaining site-to-site variability of ground motion, usually modeled via a multivariate zero-mean Gaussian distribution with covariance matrix reflecting correlation as a function of intersite distance (e.g., Jayaram and Baker, 2009).

For this case study, PGA, which is needed in the fragility function for stations, was selected as the primary *IM*. The GMPE used as the basis for the Gaussian random field (GRF) modeling of the logarithm of PGA is that by Akkar and Bommer (2010). The correlation model for intraevent residuals of PGA is that by Esposito and Iervolino (2011), which was calibrated on the data of same European strong-motion data set of the Akkar and Bommer (2010) GMPE. The correlation coefficient ρ as a function of the intersite separation distance, h, is given in Equation (4), where 13.5 is the *range* and represents the distance (in km) at which intraevent residuals may be considered uncorrelated.

$$\rho = \exp(-3 \cdot h/13.5) \tag{4}$$

In each run (that is in each simulated earthquake on the fault) and for each grid point, the mean of the logarithm of the primary *IM* was calculated via the GMPE. (In fact, given the assumption on magnitude, the mean of logarithms is the same for all runs.) The interevent residual (common to all sites) was sampled from a Gaussian distribution with zero mean and variance provided by the adopted GMPE. The intraevent residual was sampled from a multivariate Gaussian distribution characterized by the spatial correlation model expressed in Equation (4) and by GMPE's intraevent standard deviation. The resulting ground motion intensities (PGA_r) are referred to as rock/stiff-soil conditions.

The regular grid that discretizes the region occupied by the network was identified based on the correlation structure of the primary *IM* intraevent residuals. A grid size smaller than the range was chosen with the intention to represent correlation of *IMs* in one earthquake. In this case, 1-km grid spacing was selected. The value of the primary *IM* at all sites of the network (i.e., the vulnerable elements' sites) was obtained interpolating the grid values at the four closest grid points (using as weights the reciprocals of the distance of the site of interest from those points).
3. Given the primary *IM*, the secondary *IM* for each site of interest can be obtained via the mentioned conditional hazard approach. Since fragility functions for pipelines are expressed in terms of PGV, it was selected as the secondary *IM*. To obtain the conditional distribution of PGV, a GMPE for this *IM* is also required; to this aim, the work of Akkar and Bommer (2010) was considered again. Then, at each site, the realization of the logarithm of PGV_r (rock/stiff-soil conditions) was obtained sampling a normal distribution whose parameters are conditional to PGA_r. To this aim, assuming the joint normality between the logarithms of two *IMs* at the bedrock, the correlation coefficient was specifically

Table 1
Geological groups description for L'Aquila region

Class for GMPE	*Description*	*Strength parameters*	*Local lithology*
A	Rock	$c' = 15$ kPa $\phi' = 35°$	Limestones–Flysch–Debris
B	Soft rock	$c' = 0$ kPa $\phi' = 35°$	Pleistocene gravels and sands
C	Clay and silty soils	$c' = 0$ kPa $\phi' = 20°$	Holocene silts and sands

estimated starting from the data set used for the Akkar and Bommer (2010) GMPE.

4. To account for local site conditions, GMPE-based amplification factors were considered. To this aim, each site of the network was characterized according to the site classification scheme adopted by the employed GMPE, starting from geological analysis of the region described in 5. This allows obtaining PGA_s and PGV_s.

5. Regarding PGD, the landslide potential of the L'Aquila region, according to the HAZUS (FEMA, 2004) procedure was evaluated (no significant liquefaction potential was found in the region, and coseismic surface ruptures were neglected). A landslide-susceptibility map of the L'Aquila region, based on the lithological groups, slope angles, and groundwater conditions, was obtained for the purposes of this study starting from the methodology formulated by Wilson and Keefer (1985) and reported in HAZUS.

To this aim, more than 40 different outcropping lithological formations were detected in the region of interest starting from 1:50,000 scale ISPRA geological maps (http://www.isprambiente.gov.it/). The quaternary deposits and the underlying mesocenozoic formations were then grouped into three main subsoil classes based on the lithological description suggested by HAZUS. The subsoil classes are reported in Table 1, with the description of each class and the related indicative values of strength parameters (the cohesion, c', and the friction angle, ϕ').

This simplistic approach may be justified considering the regional scale of the performed risk analysis. In fact, it was adopted due to unavailability of *in situ* and laboratory test data about strength characteristics of the quaternary deposits located in the region where the network deploys (i.e., the Aterno river valley). They are mainly constituted by a depositional sequence of silt, sand, conglomerates, and gravels, as well as talus debris and debris alluvial fans covering the foot of the valley flanks: all granular hard-to-sample materials.

The calcareous and flysch deposits, mesocenozoic in age, forming the ancient and well-lithified bedrock were put into class A together with *quaternary* cemented breccias. Soils included in class A are assumed to be characterized by c' not lower than 15 kPa and by ϕ' higher than 35°. Class B comprises the quaternary clastic deposits of the region. In particular: conglomerates, gravels, slope debris, sands, and locally clay and silt. Following HAZUS indication, this class of soil is characterized by a null value of cohesion but by a rather high friction angle. Finally, in class C, all the lithotypes (late *Pleistocene-Holocene* age), present in the shallowest layers (10–15 m deep) of the central part of the Aterno river valley, were included. They are mainly made up of silts and clays; nevertheless, thin layers of sands and peats are also present. The strength properties are surely worse if compared to A and B groups so that this class was characterized by zero value of cohesion and friction angles not exceeding 20°.

The slope angle map was generated from topographic data, and slope classes were defined: <5°, 5°–10°, 10°–15°, 15°–20°, 20°–30°, 30°–40°, >40°. In particular, starting from a topographic 1:25,000 map (Istituto Geografico Militare; http://www.igmi.org/prodotti/cartografia/carte_topografiche), a digital elevation model (DEM) of the studied area was obtained with a grid resolution of 40×40 m^2 and a height resolution of 7 m. The DEM allowed the obtaining of the slope angle map, showing that in the city center, the gas network is located in flat areas, whereas in the surrounding small villages, the network crosses slopes.

Bounding groundwater conditions were assumed either dry or wet conditions. Since very limited information was available during the study about groundwater table, a dry state was attributed to the outcropping rock while wet conditions were assigned to B and C soil classes.

Ten susceptibility categories (measured on a scale of *I* to *X*, with *I* being the least susceptible) are considered in the HAZUS procedure, as a function of slope angle, groundwater conditions, and lithological classification. Each of them is characterized by a value of critical acceleration, k_c, ranging from 0.05 g to 0.6 g. (The HAZUS procedure does not account for the strength parameters assigned to each class to compute a static safety factor or to evaluate the critical acceleration.)

Overlying the slope angle, groundwater, and lithology class maps, it was possible to draw a map of the landslide susceptibility, which was finally transformed, into the critical acceleration map shown in Figure 3, where the white color corresponds to the nonsusceptible areas; i.e., those characterized by slope angle lower than 5°.

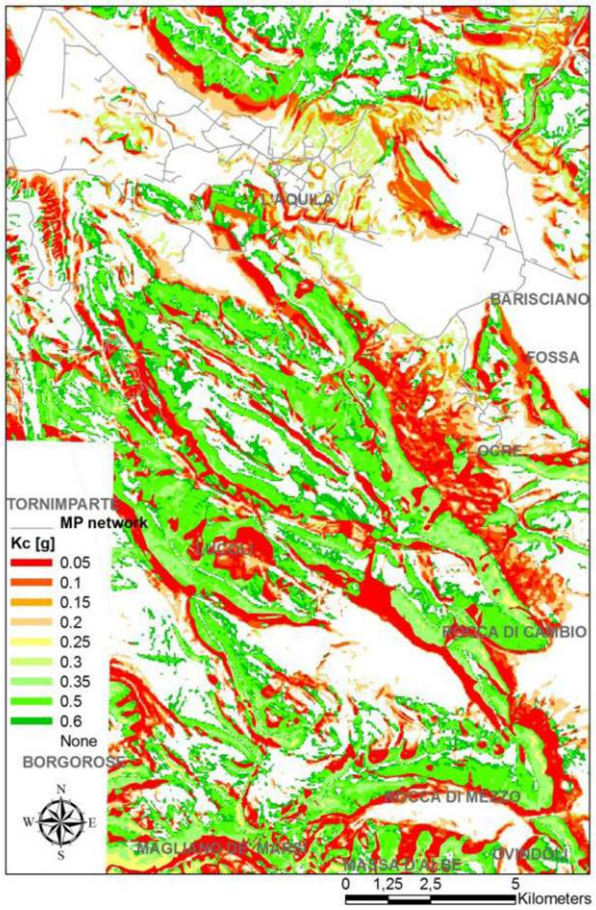

Fig. 3. Critical acceleration map for the Aterno river valley, the L'Aquila region where the network deploys.

The k_c map is to be intended as a *slope vulnerability map*, since, for a given earthquake, permanent displacements occur or not in a susceptible deposit, with probability P^*_{land} in those cases in which PGA_s exceeds k_c. This twofold condition is to account for the conservative nature of the Wilson and Keefer (1985) model, which is used in the procedure to determine the extension of the landsliding zone. In fact, the simplified approach used herein does not allow the evaluation of the extension of the landslide, but to associate, to each susceptibility category, a percentage of map area having a landslide-susceptible deposit, starting from the values proposed by Wieczoreck et al. (1985). In the methodology used herein, such values are used as probabilities of observing landsliding at a site, given that PGA at the site exceeds the critical acceleration (Weatherill et al., 2014).

In each run, the resulting displacement from PGD hazard (indicated with the same acronym for simplicity) in centimeters is finally calculated via the Saygili and Rathje (2008) empirical model, expressed in Equation (5). Such an equation, providing the conditional mean of the logarithms, is based on the computation of rigid sliding block displacements expressed as a function of the ratio between the critical acceleration k_c and the expected acceleration at surface. The model is also characterized by a residual with a standard deviation $\sigma_{\ln(PGD)}$.

$$\ln(PGD) = 5.52 - 4.43 \cdot \left(\frac{k_c}{PGA_s}\right) - 20.39 \cdot \left(\frac{k_c}{PGA_s}\right)^2 + 42.61 \cdot \left(\frac{k_c}{PGA_s}\right)^3 - 28.74 \cdot \left(\frac{k_c}{PGA_s}\right)^4 + 0.72 \cdot \ln(PGA_s) \quad (5)$$

3.2.2 Seismic vulnerability and performance assessment. To estimate earthquake-induced damage, *IMs* were related to system component damage via fragility models. For buried pipelines, Poisson repair rates functions of PGV_S and PGD were selected in ALA (2001) for each pipe typology (steel and HDPE) and diameter. In fact, an analysis of the damages to the pipelines in the L'Aquila 2009 earthquake led to conclude that these models could be a viable option to model vulnerability in the seismic risk analysis of the network; see Esposito et al. (2013) for details.

The fragility relations are indicated in Equations (6) and (7), where R_R is expressed in 1/km, PGV_S and PGD are given in cm/s and m, respectively, and K_1 and K_2 represent the modification factors according to pipe material and diameter. At each location, and in each event (i.e., run within the simulation), the rate is taken to be the largest between that obtained for PGV and PGD, and multiplied by 0.2 and 0.8, respectively, because only breaks are considered in the connectivity analysis.

$$R_R = K_1 \cdot 0.002416 \cdot PGV_s \quad (6)$$

$$R_R = K_2 \cdot 11.223 \cdot PGD^{0.319} \quad (7)$$

Although the vulnerability of RGs was neglected (also because no fragility curves are available in the literature to the knowledge of the authors), for the M/R stations, lognormal fragility curves for unanchored compressor stations (FEMA, 2004) were adopted. These have median equal to 0.77 g and 0.65 standard deviation (of the logarithms). Vulnerability to geotechnical hazards of the M/R stations was not considered because geotechnical analysis resulted in negligible susceptibility of the corresponding sites.

DSs to consider are strictly related to the objective of the analysis. In this case, a connectivity analysis was performed; i.e., the system is considered functional if

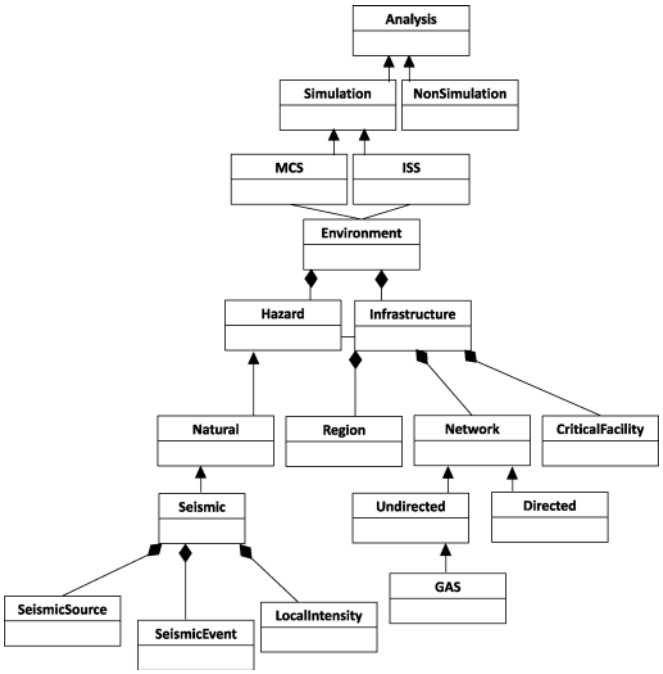

Fig. 4. Simplified version of the class diagram implemented in the OOFIMS software.

RGs remain accessible from at least one M/R station. To this aim, it was assumed that a pipe segment cannot deliver gas when the segment has at least one break, while for the supply node, it was assumed that it loses its connectivity when it is in *extensive* DS, according to the adopted fragility model.

3.3 Object-oriented software for risk analysis of lifelines

The described models were implemented in the object-oriented OOFIMS software developed by the authors (Franchin and Cavalieri, 2013) for the seismic risk assessment of interconnected infrastructural systems.

According to the OOP, the risk assessment is described as a set of objects that interact with each other. Objects are *instances* (i.e., concrete realizations) of *classes* (i.e., templates for all objects with the same set of properties and methods). Each class is defined by its *attributes* (properties of all objects from the class) and *methods* (actions that objects from the class can perform).

Figure 4 shows a simplified version of the class diagram implemented in the software where each class is represented with two boxes: the first one for the name and the second one to list all methods of the class (in the figure, since the number of methods for each class is large, the second box is left empty).

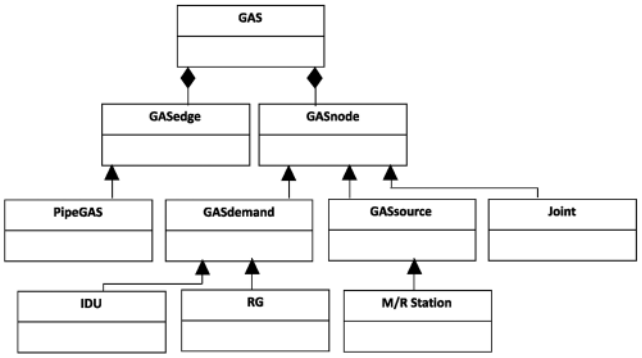

Fig. 5. Class diagram for the gas distribution network.

The first class, *Analysis*, is the generalization of all possible analysis methods (i.e., it is an abstract class). In this case, it generalizes the *Simulation* and *NonSimulation* abstract classes. The implemented portion of the model includes only the *Simulation* class, which is the generalization of two subclasses, MCS and ISS, the latter acronym standing for importance sampling simulation (e.g., Pinto et al., 2004).

An analysis is carried out on the *Environment* that is where *Hazards* act upon the *Infrastructure*. The *Hazard* abstract class is the generalization of the *Natural* class, containing environmental hazards such as the seismic one.

The *Seismic* hazard, in turn, is modeled as the composition of three classes: one class for seismic sources characterization (*SeismicSource*), one for the description of the seismic event in terms of magnitude and hypocenter (*SeismicEvent*), and one for evaluation of the seismic input in terms of TGD and PGD (*LocalIntensity*).

The *Infrastructure* class is made up of three classes: the *Region* class, the *CriticalFacility* class, and the *Network* class, that is generalization of all types of networks (*Directed* and *Undirected*).

For the purpose of this study, the model was enhanced with the *GAS* class that is considered a subclass of the *Undirected* abstract class because the gas distribution system is modeled as an undirected graph. The *GAS* class (Figure 5) is the composition of the *GASedge* and *GASnode* abstract classes, the first of which is the generalization of the *PipeGAS* class, while the second is the generalization of the *GASdemand*, *GASsource*, and *Joint* classes.

The *Joint* class represents all nodes used to reproduce the geometry of the system, the *GASsource* class represents M/R stations that are used to connect the distribution MP network to the HP transmission lines, and the *GASdemand* is the generalization of *IDU* class and *RG* class. The *IDU* class represents the node directly connected with end users in the low-pressure network,

while the *RG* class represents RGs that are considered final nodes when only the MP network is analyzed.

To evaluate the state of the network and of each component of the gas system, for each class methods and attributes were defined. Attributes refer to properties that describe the whole system and each component. Possible attributes for the *GAS* class are, for example, the number of links and nodes present in the system, as well as the list of sites where vulnerable elements are located. Attributes for links and nodes include, among others, geographical coordinates, site class, material, and other data necessary as an input to compute fragility and component performance measures. Methods, on the other hand, refer to functions used to evaluate the state of the network or of each component of the system. For example, methods include functions to evaluate the accessibility of demand nodes, based on the network damage for the generic event.

For the implementation of the network into the software, it was decided to simplify the analysis reducing the amount of data, without compromising the nature of the study; i.e., the application to a real case. In fact, to completely reflect the actual geometry of the network, more than 1,000 joint nodes should be implemented into the network model. This would have resulted in large computational demand impairing feasibility of MCS. Therefore, a data reduction process was carried out considering: (i) removal of all *dead ends* (i.e., pipes that are not carrying gas to stations or end users); (ii) simplification of the geometry merging adjacent pipes with the same geometrical and material properties. The resulting network is composed of 602 nodes (3 sources, 209 RGs, and 390 joints) and 608 links.

4 ANALYSIS AND RESULTS

According to the flowchart of Figure 6, the simulations were carried out to evaluate the statistics of the chosen PIs, given the occurrence of an earthquake on the fault. The number of runs of the simulation (2,000) was defined to yield stable estimates of the mean for all considered PIs and also to observe at least 10 occurrences in each of the 10 intervals considered for the PIs (i.e., 10 bins equally spaced and ranging from 0 to 1). Results indicate that the expected value of CL given the occurrence of an earthquake is 0.66; i.e., it is expected that the average reduction in the ability of demand nodes to be connected to M/R stations is 66% when a M_w 6.3 event occurs on the Paganica fault. For the SR indicator, it is expected that 68% of demand nodes receive gas accounting for the importance level related to the nominal flow of the demand nodes.

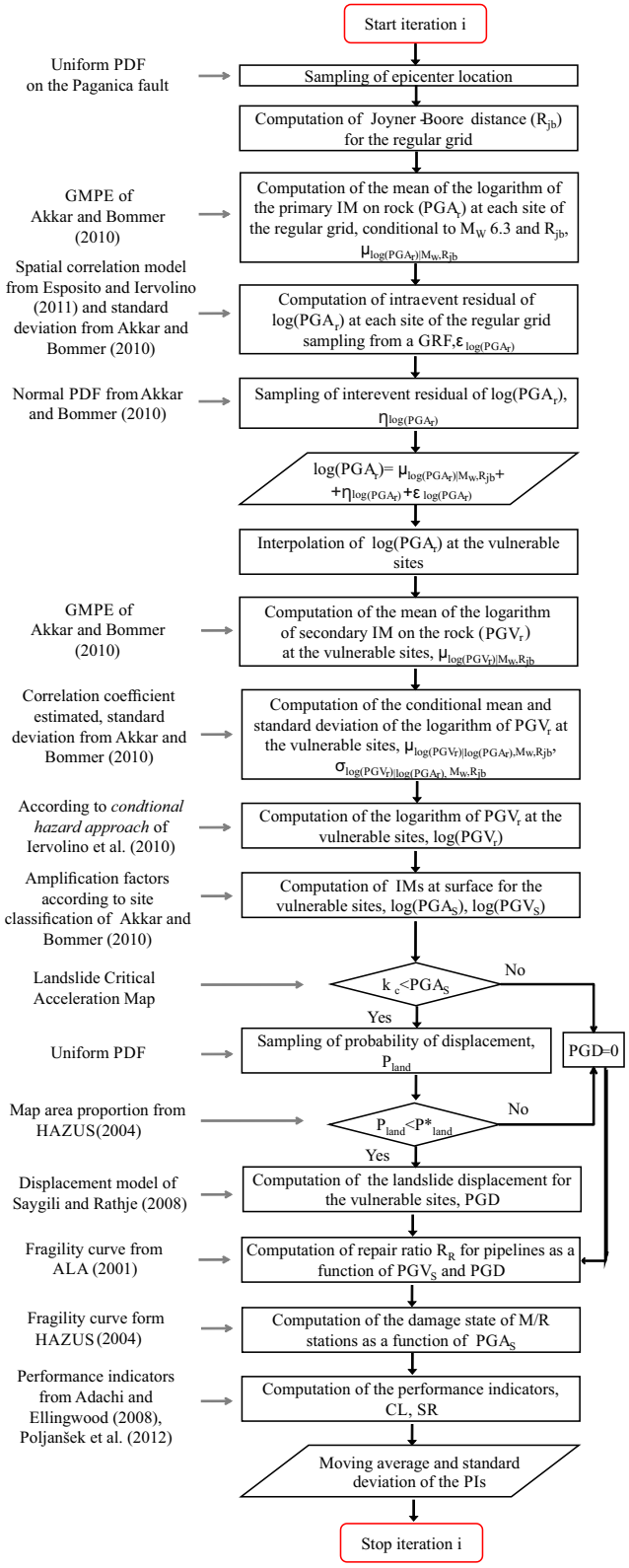

Fig. 6. Flowchart of the *i*th run in seismic risk analysis via MCS.

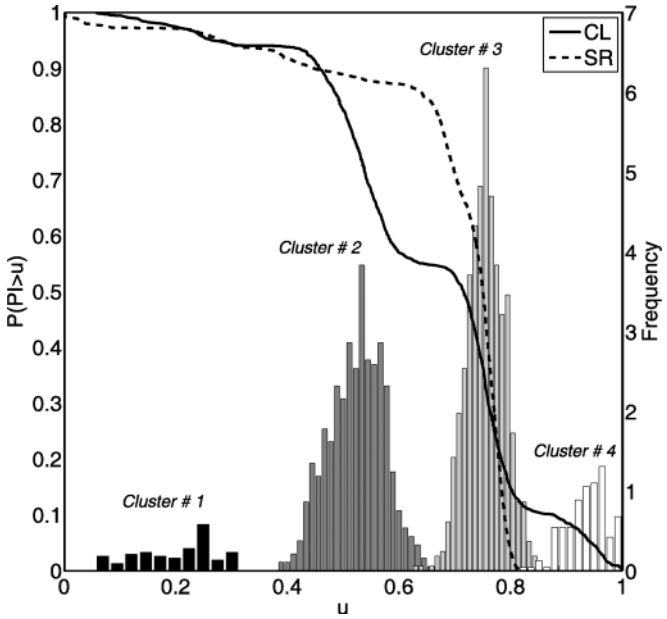

Fig. 7. Complementary cumulative distribution of CL and SR, and frequency histogram of CL with indications of clusters.

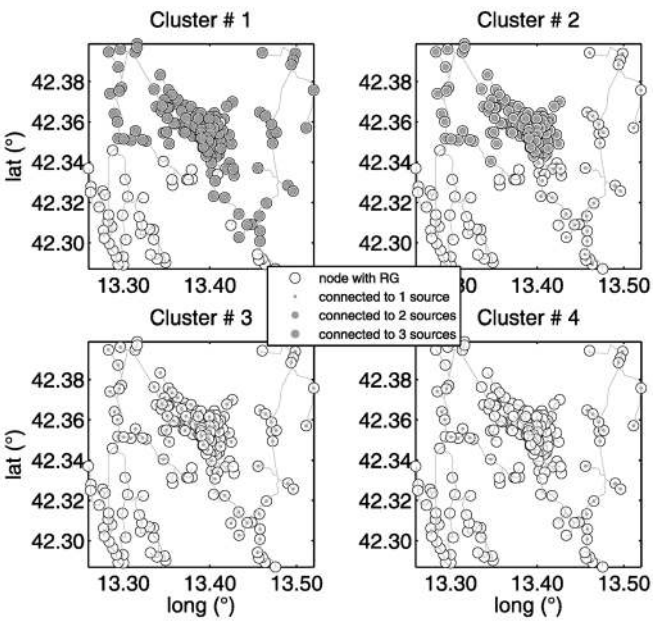

Fig. 8. Closest damage map to the centroid of each cluster.

More insight can be gained inspecting the probability of exceeding a predefined level u of performance that is the complementary cumulative distribution function (CCDF) of the chosen PIs; Figure 7. (These distributions, multiplied by the rate of occurrence of the simulated earthquakes, provide the annual rate of exceedance of the PIs, a measure of seismic risk for the infrastructure.) It may be observed from the "steps" in the CL curve that the CL is characterized by a multimodal distribution (confirmed by the frequency histogram shown in the same figure, highlighting the four modes), yet not exhibited by the corresponding SR curve. This different behavior is due to the different definition of the two PIs and the network configuration specific to the application case. Both CL and SR are averages weighted overall demand nodes (the RGs), but for each node, CL is discrete (depending on the number of sources connected to each node), while SR is an average of continuous values (the nominal flows) and whichever is the number of sources connected, as long as it is higher than zero, the indicator function X is equal to one. Further, the specific network configuration is such that performance loss in terms of number of connected sources to each node (which strongly influences CL but is much less relevant to SR) happens in clusters. Indeed, the 2,000 damage maps from the simulation were analyzed with a clustering algorithm. Among the available algorithms, ranging from spectral to kernel-based (e.g., Ahmadlou and Adeli, 2010) to evolutionary ones, the *k-means* (MacQueen, 1967) has been used in this work. It is a supervised clustering algorithm that partitions a set of observations into a number (defined by the analyst) k of clusters, such that the Euclidean distance (measuring the dissimilarity) between the observations within the same cluster is minimized. Since in this case, as already said, four modes are clearly observed, k has been set to 4, thus identifying four clusters. It is interesting to note how the maps in each cluster correspond very well to the portions of the frequency histogram around each of the four modes.

To better understand the reason of the multimodal distribution, Figure 8 shows a representative map in each of the four clusters (the closest to the cluster centroid): circles represent demand nodes, the inner dark circle can have zero, 1/3, 2/3, and 3/3 diameter, corresponding to the number of connected sources. One can see how cluster one (lower damage and associated CL values) is characterized by the central denser portion of the network being fully connected (the circles are completely filled). Representative maps from clusters two, three, and four (in order of increasing CL) show clearly that is "again" damage to the central denser portion that contributes more to the value of the CL indicator.

To evaluate the influence of accounting for correlation between intraevent residuals of *IMs*, the risk assessment was also performed considering intraevent residuals of PGA as uncorrelated. Results of this analysis, not shown here, yet available in Esposito (2011), indicate negligible influence of spatial correlation on the CCDFs of the considered PIs. However, this is not a general

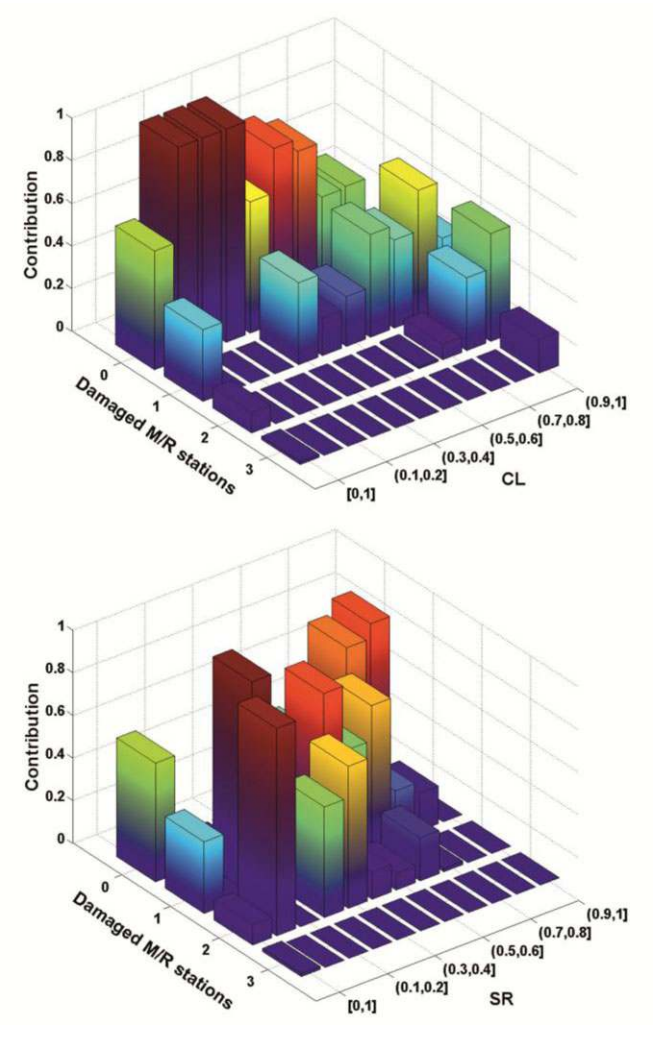

Fig. 9. Relative frequency of the number of damaged M/R stations conditional to CL (top) and SR (bottom).

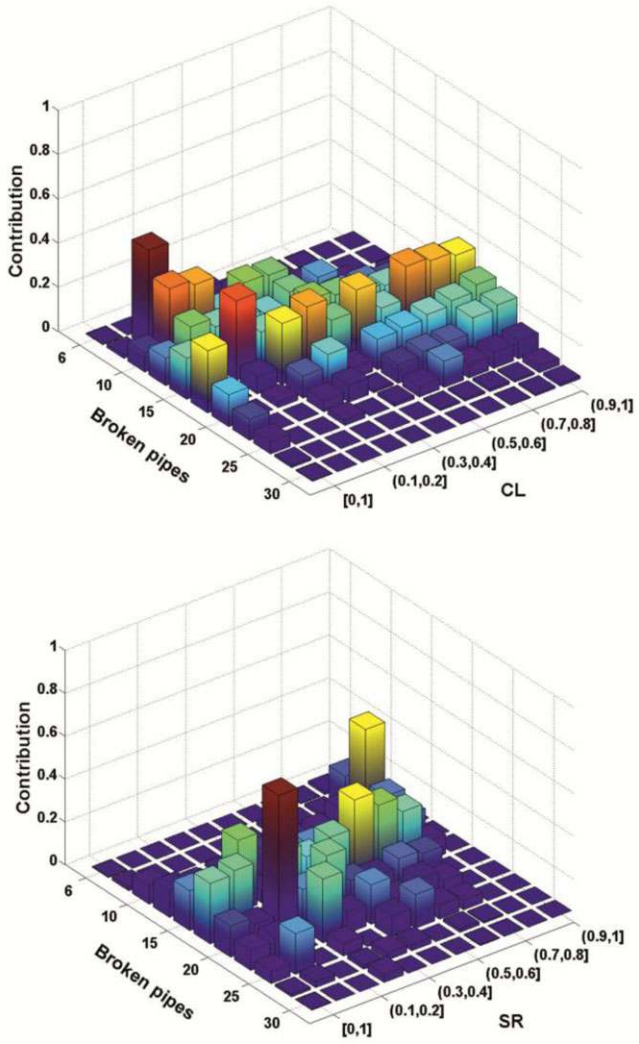

Fig. 10. Relative frequency of the number of broken pipes conditional to CL (top) and SR (bottom).

conclusion, as the effect on risk of modeling spatial correlation in random fields of ground motion intensity depends also on a number case-specific factors (see, for example, discussions in: Adachi, 2007; Adachi and Ellingwood, 2009; Esposito and Iervolino, 2011).

4.1 Disaggregation of gas network performance

To evaluate the contribution to the risk of components of the system considered vulnerable, a *disaggregation* analysis was performed. It consists of evaluating the probability distribution of a random variable (X), conditional to PI belonging to an interval between u_1 and u_2, Equation (8).

$$P\left[X = x | u_1 < PI \leq u_2\right] = \frac{P\left[X = x \cap u_1 < PI \leq u_2\right]}{P\left[u_1 < PI \leq u_2\right]} \quad (8)$$

In particular, the distribution of the number of broken pipes and damaged M/R stations, conditional to the occurrence of the two PIs in 10 intervals (equally spaced and ranging from zero to one) are shown in Figures 9 and 10. Note that in the figures, the first row in the abscissa label is the marginal probability distribution of damaged M/R stations and broken pipes.

The distribution of damaged M/R stations conditional to large losses (high values of CL and low values of SR) results as somewhat peaked toward a large number of damaged M/R stations. The distributions of number of broken pipes, conditional to the performance of the network, is somewhat more flat, with several specific numbers of breaks with comparable contribution to the PIs' intervals.

5 CONCLUSIONS

This study focused on feasibility of simulation-based seismic risk assessment of gas distribution networks, employing as much as possible state-of-the-art tools for all issues deemed relevant for this kind of system, in compliance with the PBEE framework.

The simulation procedure was developed and implemented in an object-oriented software for the risk analysis of civil infrastructures. Moreover, to deal with the issues rising in a real case, the work focused on the MP part of the L'Aquila gas system for which detailed information was retrieved.

The principal result of the risk analysis is the probability of exceeding a number of performance levels, given the occurrence of a characteristic earthquake on the fault beneath the region where the system deploys. In particular, earthquakes were generated considering the Paganica fault and characteristic earthquakes of moment magnitude 6.3. In each run, the primary ground motion intensity measure (PGA) was evaluated through a European GMPE and a European spatial correlation model; since fragilities of gas pipelines are often expressed in terms of PGV, the latter was selected as the secondary *IM*. For each site, the secondary *IM* was determined, in a probabilistically consistent manner, via the conditional hazard approach. To account for local site conditions, GMPE-based amplification factors were considered.

Regarding geotechnical hazards, resulting in the most effort-demanding issue in these kinds of problems, the landslide potential of the L'Aquila region was evaluated according to an HAZUS–like procedure. This approach appeared only feasible in consideration of the scale of the analysis and the real case study.

To estimate earthquake-induced damage, *IMs* were related to components' damage via fragility models. For buried pipelines, repair rate functions of TGD and PGD were selected for each pipe typology and diameter. For the M/R stations, a lognormal fragility curve for unanchored compressor stations was adopted, while the vulnerability of RGs was neglected.

A connectivity analysis was then performed; i.e., the system is considered functional if demand nodes continue to provide gas after the earthquake. To this aim, two connectivity-based PIs (SR and CL) were considered.

Results of the analyses indicate that the expected value of CL for the considered system, given the occurrence of an earthquake on the considered fault, is 0.66. For the SR indicator, it is expected that 68% of demand nodes receive gas accounting for the importance level related to the nominal flow of the demand nodes.

Finally, to investigate the effect of number of pipe breaks and damaged M/R stations, a disaggregation analysis of the performance was carried out.

ACKNOWLEDGMENTS

This study was partially supported by AMRA scarl (http://www.amracenter.com) in the frame of SYNER-G (seventh framework program of the European Community for research, technological development and demonstration activities; project contract no. 244061) and partially by ReLUIS, within the ReLUIS-DPC 2010–2013 research program. Authors want to acknowledge the network operator (Enel Rete Gas s.p.a.) for providing data for the characterization of the case study. Finally, Miss Racquel K. Hagen of Stanford University, who has proofread the article, is gratefully acknowledged.

REFERENCES

Adachi, T. (2007), Impact of cascading failures on performance assessment of civil infrastructure systems. Ph.D. dissertation, Georgia Institute of Technology.

Adachi, T. & Ellingwood, B. R. (2008), Serviceability of earthquake-damaged water systems: effects of electrical power availability and power backup systems on system vulnerability, *Reliability Engineering and System Safety*, **93**(1), 78–88.

Adachi, T. & Ellingwood, B. R. (2009), Serviceability assessment of a municipal water system under spatially correlated seismic intensities, *Computer-Aided Civil and Infrastructure Engineering*, **24**(4), 237–48.

Adeli, H. & Kao, W.-M. (1996), Object-oriented blackboard models for integrated design of steel structures, *Computers and Structures*, **61**(3), 545–61.

Adeli, H. & Yu, G. (1995), An integrated computing environment for solution of complex engineering problems using the object-oriented programming paradigm and a blackboard architecture, *Computers and Structures*, **54**(2), 255–65.

Ahmadlou, M. & Adeli, H. (2010), Enhanced probabilistic neural network with local decision circles: a robust classifier, *Integrated Computer-Aided Engineering*, **17**(3), 197–210.

Akkar, S. & Bommer, J. J. (2010), Empirical equations for the prediction of PGA, PGV and spectral accelerations in Europe, the Mediterranean region and the Middle East, *Seismological Research Letters*, **81**(2), 195–206.

ALA (2001), *Seismic Fragility Formulations for Water Systems*, Part 1, Guidelines, American Lifeline Alliance, ASCE.

Baker, J. & Faber, M. H. (2008), Liquefaction risk assessment using geostatistics to account for soil spatial variability, *Journal of Geotechnical and Geoenvironmental Engineering*, **134**(1), 14–23.

Banerjee, S. & Shinozuka, M. (2004), Nonlinear static procedure for seismic vulnerability assessment of bridges,

Computer-Aided Civil and Infrastructure Engineering, **22**(4), 293–305.

Cavalieri, F., Franchin, P., Buritica Cortes, J. A. M. & Tesfamariam, S. (2014), Models for seismic vulnerability analysis of power networks: comparative assessment, *Computer-Aided Civil and Infrastructure Engineering*, **29**(8), 590–607.

Chang, L. & Song, J. (2007), Matrix-based system reliability analysis of urban infrastructure networks: a case study of MLGW natural gas network, in *Proceedings of the 5th China-Japan-US Trilateral Symposium on Lifeline Earthquake Engineering*, November 26–28, Haikou, China.

Ching, J. & Hsu, W.-H. (2007), An efficient method for evaluating origin-destination connectivity reliability of real-world lifeline networks, *Computer-Aided Civil and Infrastructure Engineering*, **22**(8), 584–96.

Chioccarelli, E. & Iervolino, I. (2010), Near-source seismic demand and pulse-like records: a discussion for L'Aquila earthquake, *Earthquake Engineering and Structural Dynamics*, **39**(9), 1039–62.

Chuang, L. C. & Adeli, H. (1993), Design-independent CAD Window system using the object-oriented paradigm and HP X widget environment, *Computers and Structures*, **48**(3), 433–40.

Duenãs-Osorio, L. & Rojo, J. (2011), Reliability assessment of lifeline systems with radial topology, *Computer-Aided Civil and Infrastructure Engineering*, **26**(2), 111–28.

Eidinger, J. (1998), Water distribution system, in Ashel J. Schiff (ed.), *The Loma Prieta California Earthquake of October 17, 1989 – Lifelines*, USGS Professional Paper No. 1552-A, U.S. Government Printing Office, Washington DC, pp. A63–78.

Esposito, S. (2011), Systemic seismic risk analysis of gas distribution networks. Ph.D. thesis, University of Naples Federico II, Naples, Italy. Advisor: I. Iervolino, available at: wpage.unina.it/iuniervo.

Esposito, S., Giovinazzi, S., Elefante, L. & Iervolino, I. (2013), Performance of the L'Aquila (central Italy) gas distribution network in the 2009 (Mw 6.3) earthquake, *Bulletin of Earthquake Engineering*, **11**(6), 2447–66.

Esposito, S. & Iervolino, I. (2011), PGA and PGV spatial correlation models based on European multievent datasets, *Bulletin of the Seismological Society of America*, **101**(5), 2532–41.

FEMA (Federal Emergency Management Agency) (1992), *Earthquake resistant construction of gas and liquid fuel pipeline systems serving, or regulated by the federal government*, FEMA 233, Washington DC.

FEMA (Federal Emergency Management Agency) (2004), *Multi-hazard loss estimation methodology-earthquake model: HAZUS MR4 technical manual*, Washington DC.

Franchin, P. & Cavalieri, F. (2013), Seismic vulnerability analysis of a complex interconnected civil infrastructure, in S. Tesfamariam and K. Goda (eds.), *Handbook of Seismic Risk Analysis and Management of Civil Infrastructure Systems*, Woodhead Publishing Limited, Cambridge, UK.

Gehl, P., Desramaut, N., Réveillère, A. & Modaressi, H. (2014), Fragility functions of gas and oil networks, in K. Pitilakis et al. (eds.), *SYNER-G: Typology Definition and Fragility Functions for Physical Elements at Seismic Risk,* vol. 27*,* Geotechnical, Geological and Earthquake Engineering, Springer, Netherlands.

Hung, S. L. & Adeli, H. (1994), Object-oriented back propagation and its application to structural design, *Neurocomputing*, **6**(1), 45–55.

Iervolino, I., Giorgio, M., Galasso, C. & Manfredi, G. (2010), Conditional hazard maps for secondary intensity measures, *Bulletin of the Seismological Society of America*, **100**(6), 3312–19.

Jahani, E., Muhanna, R. L., Shayanfar, M. A. & Barkhordari, M. A. (2014), Reliability assessment with fuzzy random variables using interval Monte Carlo simulation, *Computer-Aided Civil and Infrastructure Engineering*, **29**(3), 208–20.

Jayaram, N. & Baker, J. (2009), Correlation model for spatially distributed ground motion intensities, *Earthquake Engineering and Structural Dynamics*, **38**(15), 1687–708.

Jiang, X. & Adeli, H. (2004), Object-oriented model for freeway work zone capacity and queue delay estimation, *Computer-Aided Civil and Infrastructure Engineering*, **19**(2), 144–56.

Kang, W.-H., Song, J. & Gardoni, P. (2008), Matrix-based system reliability method and applications to bridge networks, *Reliability Engineering and System Safety*, **93**(11), 1584–93.

Karim, A. & Adeli, H. (1999a), Object-oriented information model for construction project management, *Journal of Construction Engineering and Management*, **125**(5), 361–67.

Karim, A. & Adeli, H. (1999b), CONSCOM: an OO construction scheduling and change management system, *Journal of Construction Engineering and Management*, **125**(5), 368–76.

Kim, Y. & Kang, W. H. (2013), Network reliability analysis of complex systems using a non-simulation method, *Reliability Engineering and System Safety*, **110**, 80–88.

Kramer, S. L. (1996), *Geotechnical Earthquake Engineering*, Prentice Hall Inc., Upper Saddle River, NJ.

Luco, N. & Cornell, C. A. (2007), Structure-specific scalar intensity measures for near-source and ordinary earthquake ground motions. *Earthquake Spectra*, **23**(2), 357–92.

MacQueen, J. (1967), Some methods for classification and analysis of multivariate observations, in *Proceedings of the 5th Berkeley Symposium on Mathematical Statistics and Probability*, vol. 1, 281–97.

O'Rourke, M. J. & Ayala, G. (1993), Pipeline damage due to wave propagation, *Journal of Geotechnical Engineering*, **119**(9), 1490–98.

O'Rourke, M. J. & Liu, X. (1999), Response of buried pipelines subjected to earthquake effects, MCEER Monograph No. 3.

O'Rourke, T. D. & Palmer, M. C. (1996), Earthquake performance of gas transmission pipelines, *Earthquake Spectra*, **20**(3), 493–527.

O'Rourke, T. D., Toprak, S. & Sano, Y. (1998), Factors affecting water supply damage caused by the Northridge earthquake, in *Proceedings of the 6th U.S. National Conference on Earthquake Engineering EERI*, Seattle, WA.

Osiadacz, A. J. (1987), *Simulation and Analysis of Gas Networks*, 1st edn, D. and F.N. Spon Ltd, London.

Pace, B., Perruzza, L., La Vecchia, G. & Boncio, P. (2006), Layered seismogenic source model and probabilistic seismic-hazard analyses in central Italy, *Bulletin of the Seismological Society of America*, **96**(1), 107–32.

Park, J., Bazzurro, P. & Baker, J. (2007), Modeling spatial correlation for ground motion intensity measures for regional seismic hazard and portfolio loss estimation, in *Proceedings of 10th International Conference on Statistic and Probability in Civil Engineering (ICASP10)*, Tokyo, Japan.

Petersen, M. D., Dawson, T. E., Chen, R., Cao, T., Wills, C. J., Schwartz, D. P. & Frankel, A. D. (2011), Fault displacement hazard for strike-slip faults, *Bulletin of the Seismological Society of America*, **101**(2), 805–25.

Pinto, P. E., Giannini, R. & Franchin, P. (2004), *Seismic Reliability Analysis of Structures*, IUSS Press, Pavia, Italy.

Pitilakis, K., Alexoudi, M., Argyroudis, S., Monge, O. & Martin, C. (2006), Earthquake risk assessment of lifelines, *Bulletin of Earthquake Engineering*, **4**(4), 365–90.

Poljanšek, K., Bono, F. & Gutiérrez, E. (2012), Seismic risk assessment of interdependent critical infrastructure systems: the case of European gas and electricity networks, *Earthquake Engineering and Structural Dynamics*, **41**(1), 61–79.

Saygili, G. & Rathje, E. M. (2008), Empirical predictive models for earthquake-induced sliding displacements of slopes, *Journal of Geotechnical and Geoenvironmental Engineering*, **134**(6), 790–803.

Wang, Y., Au, S. & Fu, Q. (2010), Seismic risk assessment and mitigation of water supply systems, *Earthquake Spectra*, **26**(1), 257–74.

Weatherill, G., Esposito, S., Iervolino, I., Franchin, P. & Cavalieri, F. (2014), Framework for seismic hazard analysis of spatially distributed systems, in K. Pitilakis et al. (eds.), *SYNER-G: Systemic Seismic Vulnerability and Risk Assessment of Complex Urban, Utility, Lifeline Systems and Critical Facilities*, vol. 31, Geotechnical, Geological and Earthquake Engineering, Springer, Netherlands.

Wieczoreck, G. F., Wilson, R. C. & Harp, E. L. (1985), *Map of Slope Stability during Earthquakes in San Mateo County*, U.S. Geological Survey Miscellaneous Investigations, California, Map I-1257-E, scale 1:62,500.

Wilson, R. C. & Keefer, D. K. (1985), Predicting areal limits of earthquake induced landsliding, in J. I. Ziony (ed.). *Evaluating Earthquake Hazards in the Los Angeles Region*, U.S. Geological Survey Professional Paper 1360, pp. 317–45.

Youd, T. L., Hansen, C. M. & Bartlett, S. F. (2002), Revised multilinear regression equations for prediction of lateral spread displacement, *Journal of Geotechnical and Geoenvironmental Engineering*, **128**(12), 1007–17.

Yu, G. & Adeli, H. (1993), Object-oriented finite element analysis using EER model, *Journal of Structural Engineering*, **119**(9), 2763–81.

Zerva, A. (2009), *Spatial Variation of Seismic Ground Motions: Modeling and Engineering Applications*, CRC Press, Boca Raton, FL.